Aparicio Esteve, E., Hernández, A., Ureña, J., Villadangos, J.M. & Ciudad, F. 2019, "Estimation of the polar angle in a 3D infrared indoor positioning system based on a QADA receiver", in 2019 International Conference on Indoor Positioning and Indoor Navigation (IPIN), Pisa, Italy, pp. 1-8.

Available at https://dx.doi.org/10.1109/IPIN.2019.8911775

Estimation of the Polar Angle in a 3D Infrared Indoor Positioning System based on a QADA receiver

Elena Aparicio-Esteve, Álvaro Hernández, Jesús Ureña, José M. Villadangos, Francisco Ciudad
Electronics Department, University of Alcalá
Alcalá de Henares (Madrid), Spain
elena.aparicio@uah.es

***Abstract*—Three-dimension infrared positioning systems are a must on indoor local positioning systems, where those based on photodetectors are the most typically used in order not to have complex processing algorithms but a fast positioning computation. Most optical positioning systems are characterized by their low cost, low lifetime, and easy integration on the workplace. This work proposes an infrared positioning system based on four infrared LEDs and a QADA receiver. By applying encoding techniques to the infrared transmissions, the points of incidence from those transmitters on the QADA receiver are simultaneously obtained and the polar angle compensated, in order to finally estimate the receiver's position. The geometrical considerations of the system have been derived, including the polar angle and its behaviour with regard to the receiver's position, the angle of incidence and the aperture height. The proposal has been successfully validated by simulation and experimental tests, obtaining positioning errors below 10 cm.**

Keywords—Indoor local positioning system, infrareds, QADA photoreceiver.

I. INTRODUCTION

Nowadays, affordable and accurate positioning systems are highly demanded due to the development of a variety of applications and services based on positioning. Global Navigation Satellite Systems (GNSS) are clearly the most spread in outdoor environments due to its great performance in not densely populated areas. However, regarding Local Positioning Systems (LPS) in indoor areas, those based on optical, acoustic and radiofrequency technologies, among others, are the most used [1]. Although radiofrequency and acoustic technologies have accuracies in the range of centimetres [2] [1], positioning systems based on optical systems are increasing their presence in the market due to their low cost, long lifetime and easy manipulation and integration on the workplace [3], in addition to their harmless [4].

Generally speaking, optical systems use a lamp or a LED (*Light Emitting Diode*) array [5] as a transmitter, whereas at the receiver there are positioning systems based on: imaging sensors or cameras [6], which requires complex image processing algorithms that slow down the positioning computation [7]; and on photodetectors, which use photodiodes [8] or an array of photodiodes [9], to generate a current for a light impact according to the incident angle. This angle can be used to estimate the receiver's position by applying a positioning algorithm. Among these, the use of a Quadrant Photodiode Angular Diversity Aperture (QADA) in combination with an aperture [9] is highlighted due to its better angle diversity.

On the other hand, the typically used positioning techniques are: triangulation or trilateration/multilateration with Times-of-Arrival (TOA) or Time-Differences-of-Arrival (TDOA) [10], which require a strong synchronization [11]; Received Signal Strength (RSS) [12], that must consider the multipath effect to achieve accurate results, thus implying an increase in the difficulty of algorithms [13]; or Angle-of-Arrival (AOA) [3]. This last technique only requires three measures to obtain a position in three dimensions (3D), as well as no synchronization is required among transmitters [13]. Another key aspect is the medium access technique, often related to the modulation scheme used in transmissions. Although several works rely on On-Off Keying (OOK) modulations [14], due to its simplicity [15], in [16] a Binary Phase Shift Keying (BPSK) is compared with an OOK modulation, resulting in the BPSK to have the best performance.

In addition, the vast majority of infrared (IR) LPSs consider alignment between transmitter and receiver, with fixed transmitters installed in the ceiling. Furthermore, those, that consider a certain polar angle in the receiver, require accelerometers [17], several transmitters [18], and/or the combination of optical systems with other technology [19], which complicate the receiver and the processing algorithm involved. Therefore, there is a current need in the use of a simpler processing technique with a simpler receiver for indoor optical LPS.

This work presents the design and implementation of an Indoor Infrared Positioning System, which is based on four IR LED lamps as transmitters and a QADA as a receiver. A triangulation technique has been proposed to estimate the receiver's position inside a coverage area. General equations have been derived to obtain the receiver's position under a certain polar angle, according to the incidence of light and the points of incidence for the different LED projections onto the receiver's surface. An encoding scheme based on 1023-bit Kasami sequences has been proposed for every transmission coming from the LED lamps, in order to improve the system to deal with low signal-to-noise ratios (SNR) and harsh conditions, such as near-far effect and multipath. The proposal has been evaluated and successfully verified by means of simulations and experimental tests. The rest of the manuscript is organized as follows: Section II provides a general description of the system including the LED emitters and the proposed photodiode matrix, as well as a short description of the calculation of the point of incidence in the QADA receiver;

This work has been supported by the Spanish Ministry of Science, Innovation and Universities (SOC-PLC project, ref. TEC2015-64835-C3-2-R, TARSIUS project, ref. TIN2015-71564-C4-1-R), and the Youth Employment Program (PEJ2018-003459-A).

Section III details the proposed positioning algorithm; Section IV shows some simulation results, whereas Section V details the experimental results; and, finally, conclusions are discussed in Section VI.

II. General Overview of the Proposal

As has already mentioned above, the proposed indoor infrared positioning system is based on a set of four transmitters, which are placed at certain points in the ceiling, so that they cover an area where the receiver can detect their emissions and estimate its own position. A general scheme of the system is shown in Fig. 1, whereas the zoomed details of the receiver are presented in Fig. 2.

Each of the IR LED emitters are composed of an OSLON 1 PowerStar IR ILH-IW01-85SL-SC221-WIR200 [20] centred at a wavelength λ=850nm. It has a beam angle of 150º and emits a maximum of 1.27W whether a typical voltage of 3.2V is applied. Those LEDs are excited individually with a 1023-bit Kasami code c_i by using a Blueboard LPC1768-H platform. The codes c_i are BPSK modulated with a square carrier signal. On the other hand, the receiver is a QP50-6-18u-SD2 board [21], mainly composed of a QADA receiver QP50-6-18u-TO8 with a radius r=3.9mm. It provides the sum of all quadrant signals and two difference signals, bottom minus top (Y axis) and left minus right (X axis). Its responsivity at a wavelength λ=950nm is 0.65A/W.

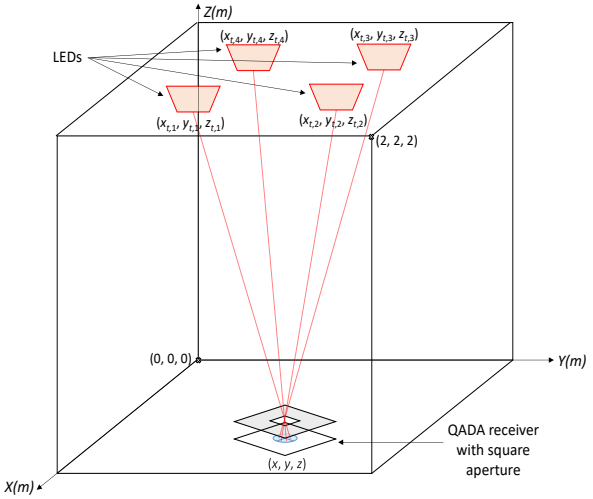

Fig. 1. Proposed positioning system with LED emitters and a photodiode array (note that elements are not to scale).

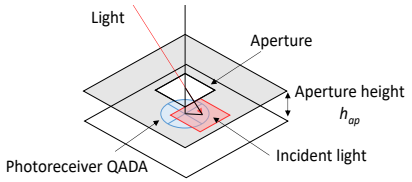

Fig. 2. Geometrical representation of the incident light in the QADA photoreceiver.

As a study case, the proposed system has been particularized hereinafter for a volume of 2mx2mx2m, where the emitters, i={1,2,3,4}, have been placed at the coordinates ($x_{t,i}$, $y_{t,i}$, $z_{t,i}$) defined in Table I.

TABLE I. IR LED coordinates in the study case considered here.

LED	Coordinates (x_t, y_t, z_t)$_i$
LED 1	(4/3 m, 2/3 m, 2 m)
LED 2	(4/3 m, 4/3 m, 2 m)
LED 3	(2/3 m, 4/3 m, 2 m)
LED 4	(2/3 m, 2/3 m, 2 m)

Two reference systems are considered in this proposal: one referred to the point of impact of the light onto the QADA receiver (x_r, y_r); and the other with regard to the position of the receiver in the whole volume (x, y, z). It is considered that there is no angle of inclination (neither in the emitters nor in the QADA receiver), but there is a certain polar angle β (angle of rotation) in the receiver. Furthermore, it is assumed that the X and Y axes of the LEDs and the QADA receiver are aligned when the polar angle is β=0º.

A. Proposed central impact point estimation at the receiver.

The operation principle of the proposal is based on the fact that the light coming from the LEDs goes through the centre of the square aperture, with a side equal to the diameter of the photoreceiver ($2 \cdot r$=7.8mm), and lights the photoreceiver as presented in Fig. 2. Note that the square aperture is installed on the receiver at a height h_{ap}=2.6mm above it.

According to the incidence angle ψ, different areas are illuminated in the different photodiodes. Fig. 3 shows the four quadrants and the area covered by the beam of light that passes through the aperture for the case of an incident ray for a certain impact point (x_r, y_r) [22]. Further details about the algorithm proposed to estimate the impact point can be found in [23] [24]. The incident light generates four different currents $i_j(t)$ for every quadrant j={1,2,3,4}.

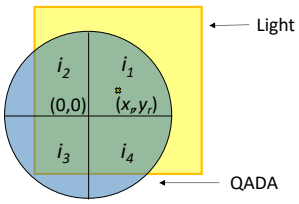

Fig. 3. Incident light in a QADA receiver through an aperture.

Note that these output voltages provided by the QADA receiver are the combination of the currents $i_j(t)$ obtained by the different photodiodes, transformed into voltages $v_j(t)$ by means of a transimpedance amplifier. Those signals are acquired in an oscilloscope Tektronix MDO4104-6 [25], and then transferred to a computer, where the received signals are processed to obtain the transmitters' point of incidence onto the QADA surface (x_r, y_r). This procedure relays on the cross correlation of the received signals, previously filtered, with the transmitted codes c_i. The resulting correlation peaks are used to estimate the signal level from each LED lamp i and then obtain the point of incidence for every code c_i onto the QADA photoreceiver surface by means of a Gauss-Newton algorithm [23] [24].

III. Proposed Algorithm

For the clarity's sake, it is considered hereinafter that there are at least three impact points $(x_r, y_r)_i$ on the QADA photoreceiver; particularly, the proposal has four LEDs, so four impact points $(x_r, y_r)_i$ are actually involved. The polar angles β_i shown in (1-4) are obtained by means of geometrical considerations, as detailed in Fig. 4.

$$\beta_1 = tan^{-1}\left(\frac{y_{r,1}-y_{r,2}}{x_{r,1}-x_{r,2}}\right) \quad (1)$$

$$\beta_2 = tan^{-1}\left(\frac{x_{r,2}-x_{r,3}}{y_{r,3}-y_{r,2}m}\right) \quad (2)$$

$$\beta_3 = \tan^{-1}\left(\frac{y_{r,4}-y_{r,3}}{x_{r,4}-x_{r,3}}\right) \quad (3)$$

$$\beta_4 = tan^{-1}\left(\frac{x_{r,1}-x_{r,4}}{y_{r,4}-y_{r,1}}\right) \quad (4)$$

Where β_i is the polar angle of the receiver with respect to the transmitter i (note that they are both aligned when β_i=0º); and $(x_r, y_r)_i$ are the coordinates of the impact points of the incident light onto the QADA receiver. Thus, it can be observed that the final polar angle β can be obtained as an average of the four different angles β_i, as presented in (5).

$$\beta = \overline{(\beta_1, \beta_2, \beta_3, \beta_4)} \quad (5)$$

Note that, although Fig. 4 represents the impact points on the first quadrant, for the location of the LED lamps in Table I, this algorithm can be easily extended to the four quadrants and it is not necessary that the impact points $(x_r,y_r)_i$ are placed in the same quadrant for the algorithm to properly work. In addition, it is assumed that the rotation of the receiver is clockwise, thus the rotation of the points of incidence is anticlockwise (see Fig. 4). It is worth mentioning that the incident points are geometrically distributed with a square shape, as the transmitters are placed in the ceiling in this case.

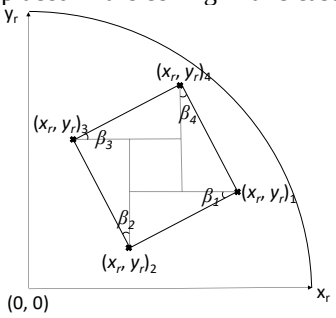

Fig. 4. First quadrant of the QADA photoreceiver with four impact points $(x_r, y_r)_i$.

The proposed algorithm is based on the analysis of the rotation of the points of incidence $(x_r, y_r)_i$, obtained for a certain polar angle β_i, with respect to the corresponding points of incidence without rotation $(x_r, y_r)'_i$ (assuming β_i=0). Note that the rotation does not imply any change in the radius of the points of incidence (see Fig. 5).

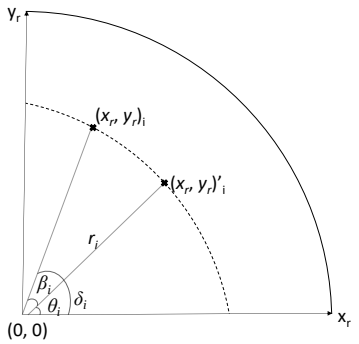

Fig. 5. First quadrant of the QADA photoreceiver with an arbitrary impact point $(x_r, y_r)_i$ and its non-rotated impact point $(x_r, y_r)'_i$.

The coordinates of the non-rotated impact point $(x_r, y_r)'_i$ are obtained as (6-7).

$$x'_{r,i} = r_i \cdot \cos(\theta_i) \quad (6)$$

$$y'_{r,i} = r_i \cdot sin(\theta_i) \quad (7)$$

Where $\theta_i = \delta_i - \beta_i$; and $\delta_i = \tan^{-1}\left(\frac{y_r}{x_r}\right)_i$.

After the non-rotated coordinates $(x_r, y_r)'_i$ are obtained, the positioning algorithm continues to obtain the final coordinates (x, y) of the receiver's position in the proposed scenario by mans of the Least Squares Estimator (LSE) [26] and the coordinate z is obtained by trigonometric considerations. More detailed information about it can be found in [23] [24].

IV. Simulated Results

For both simulations and experimental results, it is assumed that the four quadrants are exactly equal and that, under the same illuminating conditions, they generate the same currents. It is also assumed that there is no misalignment between the QADA surface and the aperture. Transmitters are located as detailed in Table I and a SNR of 10dB at the receiver is considered in simulations. No tilting in the transmitters nor in the receiver is considered, while the polar angle β is analysed.

Firstly, some simulations are performed in order to determine the absolute error of the proposed algorithm in the calculation of the polar angle β.

Fig. 6 represents the cumulative distribution function (CDF) of the absolute errors of the polar angle for β={20º, 110º, 200º, 340º} and β={30º, 60º, 120º, 300º}. It has been analysed in a grid of 2x2m every 10cm with a hundred measurements at each point with z=0m. Note that those CDFs, whose angles verify $90° \cdot n \pm \beta$ (n is an integer), have similar results and, consequently, their absolute error is also similar. It can be verified an absolute error of 1.2º in the 90% of measures for polar angles β={20º, 110º, 200º, 340º}, and 0.8º in the 90% of measures for polar angles β={30º, 60º, 120º, 300º}. Therefore, hereinafter only the first octant is analysed (from 0º to 45º), since the results can be extended to the rest of the circumference.

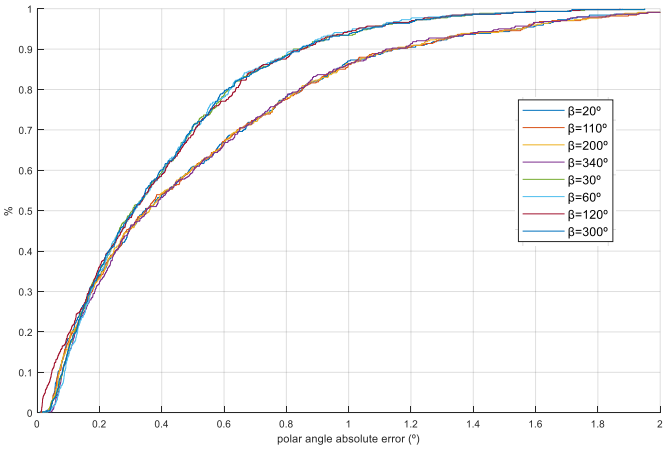

Fig. 6. Absolute error in the estimation of the polar angle β for different values at z=0 m.

In Fig. 7 the absolute errors of the polar angle β are detailed for angles in the range from 0º to 45º. Furthermore, the global absolute error in the proposed scenario, for all possible angles β, is detailed with a black line. This global error is 0.9º in the 90% of the cases. The worst performance of the algorithm occurs at β=15º when an error of 1.25º is found in the 90% of the measures, whereas the best performance is at β=45º with a 0.25º of absolute error.

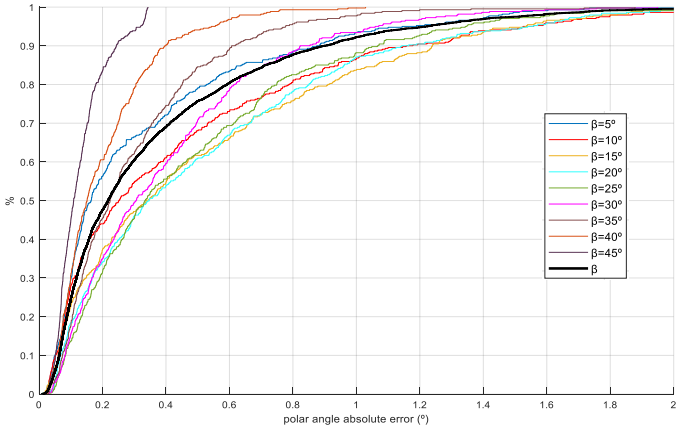

Fig.7. Absolute error in the estimation of the polar angle for values β={5º,10º,15º,20º,25º,30º,35º,40º,45º} at z=0 m.

Fig. 8 presents the error in the estimation of the polar angle for a particular value β=30º, depending on the receiver's position in the area under coverage. Two heights, z=0m and z=1m, are considered, whereas the receiver is placed along the X and Y axes, always with the same angle β=30º. The red crosses represent the projected position of the transmitters in the XY plane. The polar angle β=30º is selected due to its proximity to the global error CDF in Fig.7. It is possible to distinguish a rotated cross in Fig. 8 where absolute errors are higher and close to 1º. This cross is actually rotated 30º, the same as the polar angle β=30º. This is due to the fact that some uncertaintity appears when coordinates x_r and/or y_r are close to 0, since in these cases the point of incidence in the QADA surface is near to the axes of the photoreceiver. Note that these higher errors are strongly dependent on the selected polar angle β and appear for any value of β.

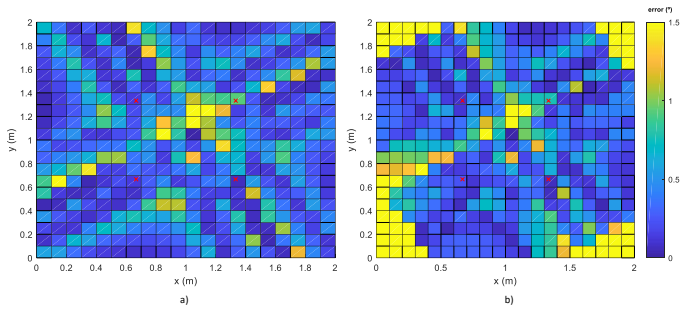

Fig. 8. Absolute errors in the estimation of the polar angle, depending on the coordinates x_r and y_r, with β=30º at: a) z=0 m; b) z=1 m

It is also possible to observe in Fig. 8 that, apart from corners at z=1m where no signal is detected and positioning is not possible, the worst performance is obtained for z=0 m. Therefore, the absolute errors of the estimated coordinates (x, y, z) are analysed by means of a CDF in Fig. 9 for a polar angle β in the first octant, every 5º, at z=0 m. In the 90% of the measurements, the absolute error in the coordinates x and y is 0.12m, whereas it is 0.32m for the coordinate z. Note that those absolute values are the same for any polar angle β considered since they converge in the CDFs for the 90% of the measurements in all cases considered here. Thus, it is worth mentioning that an increase of 1º in the absolute error of the polar angle (the difference between the worst and the best cases in Fig. 7) is negligible from the point of view of the positioning algorithm, with similar results in all the coordinates in Fig. 9.

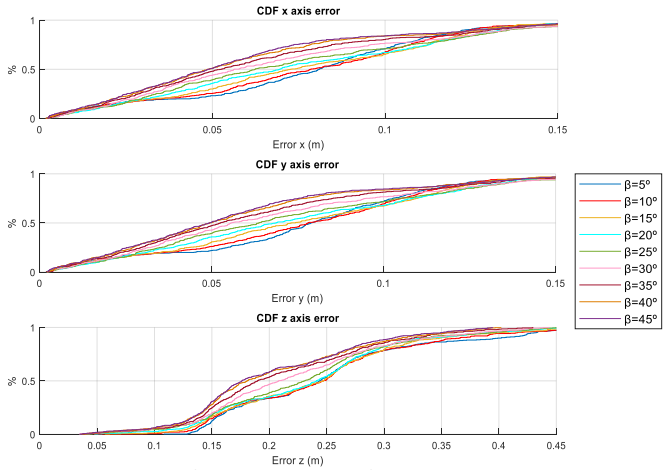

Fig. 9. CDF of the absolute errors for coordinates (x, y, z) at z=0m, depending on the polar angle β.

Finally, a grid of 2x2x2m in steps of 50 cm is detailed, with a total of 25 points of measurement represented as black crosses, as is shown in Fig. 10. The polar angles considered here are β={5º, 10º, 15º, 20º, 25º, 30º, 35º, 40º, 45º} at z=0 m. Thus, all polar angles, from 0º up to 360º, are considered, as previously demonstrated. Similarly, the absolute errors of the coordinates x, y and z for those points are detailed as CDF in Fig. 11.

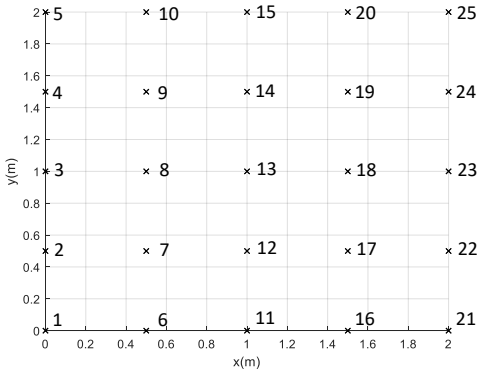

Fig. 10. Scheme of the analysed points in a grid of 2x2x2 m.

Fig. 11 provides a good understanding of the positioning algorithm, which strongly depends on the position where the receiver is located. Those blue curves in the CDF of the absolute error for the coordinate *x* are the ones corresponding to those points in the centre of the X axis, and, therefore, they have the best performance with less than 4cm of absolute error in the 90% of the measurements. On the other hand, the green and orange curves are those points in the region between the centre and the border of the X axis, reaching errors of around 8cm for the coordinate *x*. Finally, the worst absolute errors are found at the corners of the X axis for red and pink curves. Coordinates *y* and *z* behaves similarly.

Note that there is a slight difference in the behaviour of the CDFs between Fig. 9 and Fig. 11, due to the points considered in the simulation. In Fig. 9 all points in the grid were simulated, whereas in Fig. 11 only 25 points are taken into account, with a majority of those in the borders of the grid.

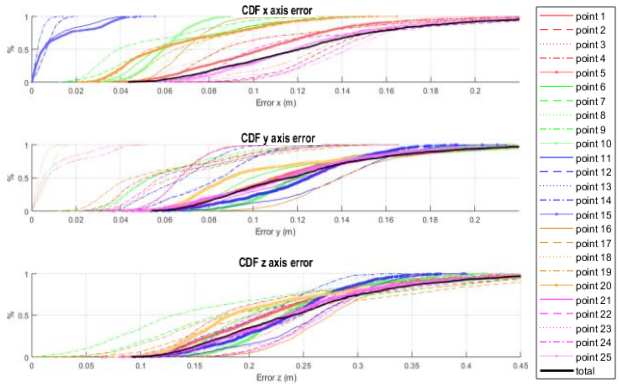

Fig. 11. CDF of the absolute error of the coordinates *x*, *y*, *z* for the 25 analysed points at *z*=0 m.

V. Experimental Results

The experimental setup has been assembled according to the scheme in Fig. 1, where the four transmitters are at a distance of 2 m from the QADA photoreceiver, located in plane *z*=0 m. Note that the noise from other lamps or the sunlight is discarded by means of the cross correlation techniques with the transmitted codes c_i, so that they can be turned on during experiments. The analysed area covers a 2mx2m surface. A certain polar angle β have been set for every points; particularly, the considered polar angles β are 5º and 45º, since it can be derived from Fig. 9 that the worst performance is obtained for β=5º whereas the best one is for β=45º.

Fig. 12 is a zoom from Fig. 10, where the five points considered actually represent the behaviour of the algorithm in one quadrant of the proposed space. It is possible to extend the following results to the rest of the grid. Measurements have been acquired up to 50 times per polar angle β={5º,45º} and per point. Those corresponding to β=5º are plotted in blue, whereas those for β=45º are in violet. The black crosses are the projection of the transmitters' position in the XY plane and the red crosses are the ground-truth. An error ellipse is also plotted with a 95% of confidence for each point in the XY plane.

It is worth mentioning that the best position estimates are obtained when the QADA axes are perpendicular to the transmitters' axes. Therefore, at points 1 and 2, the angle β=45º has lower positioning errors than β=5º, and the opposite behaviour is found at points 3, 4 and 5. Furthermore, the area around the centre requires lower polar angles β to achieve the same positioning error than in the borders of the surface for higher polar angles.

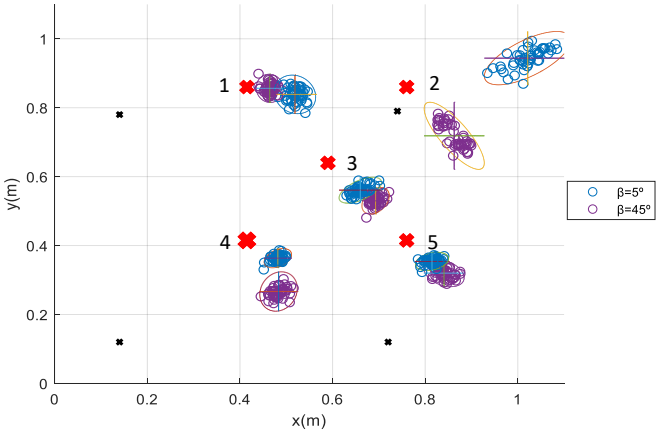

Fig. 12. Experimental position estimates at *z*=0m for β={5º, 45º}.

At this point, it is convenient to remember that all the previous results have been obtained for an aperture height h_{ap}=2.6mm. Nevertheless, the accuracy obtained in the determination of this height is key for the estimation of coordinate *z*, which is carried out by geometrical considerations [23] [24]. In order to analyse this influence, the errors obtained for the coordinate *z* at different aperture heights h_{ap} are detailed in Fig. 13. It is possible to observe that different aperture heights h_{ap} should be considered in order to achieve minimum errors in the coordinate *z* for different angles and points.

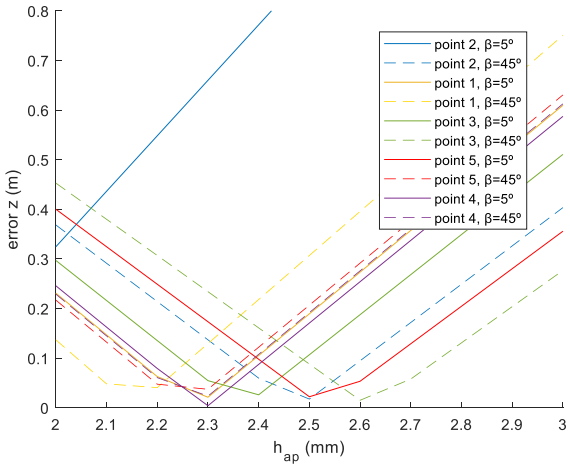

Fig. 13. Absolute error in the estimation of coordinate *z*, depending on the aperture height h_{ap}.

In this way, the aperture height is considered to be hereinafter h_{ap}=2.37mm, thus minimizing the coordinate *z* error. Table II details the averaged absolute errors and the standard deviation obtained for points in Fig. 12 with that aperture height h_{ap}.

TABLE I. AVERAGED ABSOLUTE ERROR AND STANDARD DEVIATION FOR THE CONSIDERED POINTS, ASSUMING h_{ap}=2.37mm.

		Averaged absolute error (cm)			**Standard deviation (cm)**		
	Polar angle *β*	**X axis**	**Y axis**	**Z axis**	**X axis**	**Y axis**	**Z axis**
Point 1	5º	10.38	2.27	6.78	1.6	2	3.61
	45º	4.92	1.18	10.79	1.04	1.47	4.14
Point 2	5º	15.47	13.1	21.14	6.59	11.08	29.46
	45º	10.27	14.14	4.96	2.32	3.48	4.67
Point 3	5º	8.93	9.92	9.92	2.1	2.7	3.41
	45º	10.29	11	2.67	1.06	1.38	2.56
Point 4	5º	6.67	5.16	4.14	1.06	0.99	4.01
	45º	6.83	14.83	4.2	1.45	2.04	5.7
Point 5	5º	5.47	6.11	5.77	1.29	0.95	7.42
	45º	8.07	9.5	2.94	1.55	1.41	3.81

All the points present a low standard deviation, with values around 2cm with the exception of point 2 with a polar angle of 45º for coordinate *z*. In addition, the difference in absolute values between the best and the worst polar angle, β=5º and β=45º respectively, for each point, is nearly doubled with minimum values around 5cm and maximum values around 11cm. Point 2 presents the highest errors due to the fact that it is the one located near the corner of the grid, where the transmissions arrive with the highest angle of incidence.

Note that the averaged absolute error and the standard deviation of the results obtained for coordinate *z* are strongly dependent on the aperture height h_{ap}, as well as on the incident angle; therefore, a small error in the measurement will provide large errors in this coordinate as detailed in Fig. 13.

Similarly to Fig. 11, Fig. 14 plots the CDF of the experimental results detailed in Table II. Note that most points are below 10cm of absolute error at the 90% of the cases, whereas those curves with the highest errors correspond to the points with the worst polar angle possible and at the corners of the grid.

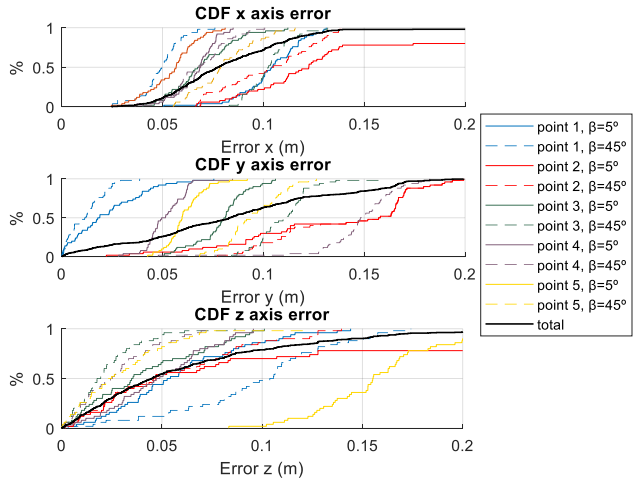

Fig. 14. CDF of the absolute error of the coordinates *x*, *y*, *z* for the five experimentally analysed points at *z*=0m.

VI. CONCLUSIONS

This work presents a study of a 3D infrared indoor positioning system, based on four infrared LEDs working as transmitters and a quadrant photodiode as receiver. The receiver identifies the transmissions from each LED by means of an encoding scheme based on 1023-bit Kasami sequences. The points of incidence of these emissions on the QADA receiver are processed to estimate the polar angle of the receiver, as well as the receiver's local position by means of geometrical considerations. The proposal has been evaluated and successfully verified by means of simulations and experimental results The obtained results details a general absolute error of 0.9º in the estimation of the polar angle, and 12cm of absolute error in the receiver's coordinates (*x*, *y*) in the 90% of the measures carried out in a 2x2x2m test scenario. The strong dependence of the obtained results with the incidence angle has also been proven, and consequently, the direct dependence with the location of the receiver in the proposed scenario for different polar angles. Errors in the range of 5-10cm are achieved in the proposed test scenario, with standard deviations of 2cm.

REFERENCES

[1] J. Ureña, A. Hernández, J. J. García, J.M. Villadangos, M.C. Pérez, D. Gualda, F. J. Álvarez, and T. Aguilera, "Acoustic Local Positioning With Encoded Emission Beacons," *Proceedings of the IEEE*, vol. 106, no. 6, pp. 1042-1062, 2018.

[2] A. Lindo, E. Garcia, J. Ureña, M. C. Perez, A. Hernandez, "Multiband waveform design for an ultrasonic indoor positioning system," IEEE Sensors Journal, vol. 15(12), pp. 7190-7199, 2015.

[3] C. Wang, L. Wang, X. Chi, S. Liu, W. Shi, and J. Deng, "The research of indoor positioning based on visible light communication," *China Communications*, vol. 12, no. 8, pp. 85-92, 2015.

[4] T. H. Do, and M. Yoo, "Performance Analysis of Visible Light Communication Using CMOS Sensors," Sensors, vol. 16(3), no. 309, pp. 1-23, 2016.

[5] F. Belloni, V. Ranki, A. Kainulainen and A. Richter, "Angle-based indoor positioning system for open indoor environments," *2009 6th Workshop on Positioning, Navigation and Communication*, Hannover, 2009, pp. 261-265.

[6] H. Santo, T. Maekawa and Y. Matsushita, "Device-free and privacy preserving indoor positioning using infrared retro-reflection imaging," *2017 IEEE International Conference on Pervasive Computing and Communications (PerCom)*, Kona, HI, 2017, pp. 141-152.

[7] P. H. Pathak, X. Feng, P. Hu, and P. Mohapatra, "Visible Light Communication, Networking, and Sensing: A Survey, Potential and Challenges," *IEEE Communications Surveys & Tutorials*, vol. 17, no. 4, pp. 2047-2077, 2015.

[8] Y. Cai, W. Guan, Y. Wu, C. Xie, Y. Chen, and L. Fang, "Indoor High Precision Three-Dimensional Positioning System Based on Visible Light Communication Using Particle Swarm Optimization," *IEEE Photonics Journal*, vol. 9, no. 6, pp. 1-20, 2017.

[9] S. Cincotta, C. He, A. Neild, and J. Armstrong, "High angular resolution visible light positioning using a quadrant photodiode angular diversity aperture receiver (QADA)," Optics Express, vol. 26, no. 7, pp. 9230-9242, 2018.

[10] T. Q. Wang, Y. A. Sekercioglu, A. Neild, and J. Armstrong, "Position Accuracy of Time-of-Arrival Based Ranging Using Visible Light With Application in Indoor Localization Systems," *Journal of Lightwave Technology*, vol. 31, no. 20, pp. 3302-3308, 2013.

[11] G. Berkovic and E. Shafir. "Optical methods for distance and displacement measurements," Advances in Optics and Photonics, vol. 4, pp. 441-471, 2012.

[12] F. Alam, M. T. Chew, T. Wenge and G. S. Gupta, "An Accurate Visible Light Positioning System Using Regenerated Fingerprint Database Based on Calibrated Propagation Model," in *IEEE Transactions on Instrumentation and Measurement*, 2018.

[13] H. Steendam, T. Q. Wang, and J. Armstrong, "Theoretical Lower Bound for Indoor Visible Light Positioning Using Received Signal Strength Measurements and an Aperture-Based Receiver," *Journal of Lightwave Technology*, vol. 35, no. 2, pp. 309-319, 2017.

[14] Z. Li, L. Feng, and A. Yang, "Fusion Based on Visible Light Positioning and Inertial Navigation Using Extended Kalman Filters," Sensors, vol. 17, no. 5, pp. 1093. 2017.

[15] M. Ijaz, O. Adebanjo, S. Ansari, Z. Ghassemlooy, S. Rajbhandari, H. Le Minh, A. Gholami and E. Leitgeb, "Experimental Investigation of the Performance of OOK-NRZ and RZ Modulation Techniques under Controlled Turbulence Channel in FSO Systems," IEEE Transactions on Instrumentation and Measurement, 2010.

[16] E. Shinwasusin, C. Charoenlarpnopparut, P. Suksompong and A. Taparugssanagorn, "Modulation performance for visible light communications," *2015 6th International Conference of Information and Communication Technology for Embedded Systems (IC-ICTES)*, pp. 1-4, 2015.

[17] K. Kalischewski, D. Wagner, J. Velten and A. Kummert, "Orientation and positioning with inertial sensors for walking frame guidance," *2015 IEEE 9th International Workshop on Multidimensional (nD) Systems (nDS)*, 2015, pp. 1-5.

[18] Zhu, Bingcheng & Cheng, Julian & Wang, Yongjin & Yan, Jun & Wang, Jin-Yuan "Three-Dimensional VLC Positioning Based on Angle Difference of Arrival With Arbitrary Tilting Angle of Receiver," *IEEE Journal on Selected Areas in Communications*, vol. 36, no. 1, pp. 8-22, 2018.

[19] S. Cincotta, C. He, A. Neild and J. Armstrong, "QADA-PLUS: A Novel Two-Stage Receiver for Visible Light Positioning," *2018 International Conference on Indoor Positioning and Indoor Navigation (IPIN)*, Nantes, 2018, pp. 1-5.

[20] Oslon, Oslon PowerStar IR ILH-IW01-85SL-SC221-WIR200 series, Product Specification, 2015.

[21] First Sensor Inc., Series 6 Data Sheet Quad Sum and Difference Amplifier, Part Description QP50-6-18u-SD2, Product Specification, 2012.

[22] S. Cincotta, C. He, A. Neild, and J. Armstrong, "High angular resolution visible light positioning using a quadrant photodiode angular diversity aperture receiver (QADA)," *Optics Express*, vol. 26, no. 7, pp. 9230-9242, 2018.

[23] E. Aparicio-Esteve, A. Hernández, J. Ureña, R. Nieto, F. Ciudad, "Implementación de un Sistema de Posicionamiento con Luz Visible basado en focos LEDs y un receptor QADA", *Seminario Anual de Automática, Electrónica Industrial e Instrumentación*, Under review, 2018.

[24] E. Aparicio-Esteve, A. Hernández, J. Ureña and J. M. Villadangos, "Visible Light Positioning System based on a Quadrant Photodiode and Encoding Techniques", in *IEEE Transactions on Instrumentation and Measurement*, Under review, 2018.

[25] Tektronix. Tektronix MDO4104-6 Mixed Domain Oscilloscope, Product Specification, 2011.

[26] Y. S. Eroglu, I. Guvenc, N. Pala and M. Yuksel, "AOA-based localization and tracking in multi-element VLC systems," 2015 IEEE 16th Annual Wireless and Microwave Technology Conference (WAMICON), pp. 1-5, 2015.